

## REVIEW SUMMARY

## ELECTRON MICROSCOPY

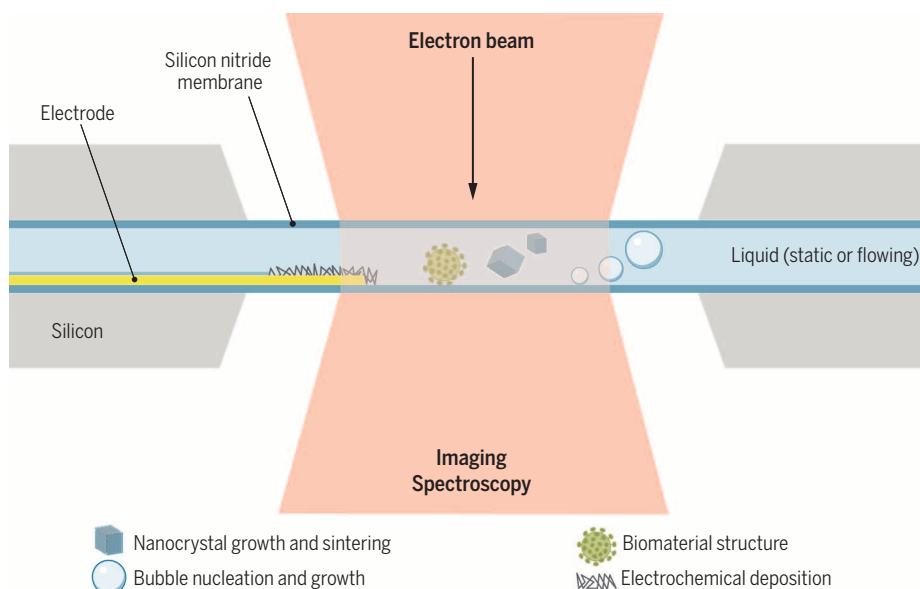
# Opportunities and challenges in liquid cell electron microscopy

Frances M. Ross

**BACKGROUND:** Transmission electron microscopy offers structural and compositional information with atomic resolution, but its use is restricted to thin, solid samples. Liquid samples, particularly those involving water, have been challenging because of the need to form a thin liquid layer that is stable within the microscope vacuum. Liquid cell electron microscopy is a developing technique that allows us to apply the powerful capabilities of the electron microscope to the imaging and analysis of liquid specimens. We can examine liquid-based processes in materials science and physics that are traditionally inaccessible to electron microscopy, and image biological structures at high

resolution without the need for freezing or drying. The changes that occur inside batteries during operation, the attachment of atoms during the self-assembly of nanocrystals, and the structures of biological materials in liquid water are examples in which a microscopic view is providing unique insights.

**ADVANCES:** The difficulty of imaging water and other liquids was recognized from the earliest times in the development of transmission electron microscopy. Achieving a practical solution, however, required the use of modern microfabrication techniques to build liquid cells with thin but strong windows. Usually



## Schematic diagram of a liquid cell for the transmission electron microscope and its application for imaging phenomena in materials science, life science, and physics.

The liquid cell is made from two vacuum-tight electron transparent membranes. In this diagram the membranes are made of silicon nitride (blue) on a silicon support (gray), although other materials are possible. A spacer layer (not shown) keeps the membranes at a controlled separation of about 100 nm to 1 μm. The cell is filled with the liquid of interest, and the liquid may be flowed using an external pump (not shown). The electron beam (pink) passes through the membranes and liquid to allow recording of images, movies, or spectroscopic data for compositional analysis. Several possible experiments are illustrated: growth of nanocrystals in solution, nucleation and growth of bubbles, imaging biological structures such as viruses in liquid water, and imaging electrochemical processes at an electrode (yellow) that is built into the liquid cell. The dimensions of the electron beam and the nanoscale objects are exaggerated for clarity.

made of silicon nitride on a silicon support, these liquid cells perform two jobs: They separate the liquid from the microscope vacuum while also confining it into a layer that is thin enough for imaging with transmitted electrons. Additional functionality such as liquid flow, electrodes, or heating can be incorporated in the liquid cell. The first experiments to make use of modern liquid cells provided information on electrochemical deposition, nanomaterials synthesis, diffusion in liquids, and the structure of biological assemblies. Materials and processes now under study include corrosion, biomolecular structure, bubble dynamics, radiation effects, and biomineralization. New window materials such as graphene can improve resolution, and elemental analysis is possible by measuring energy loss or x-ray signals. Advances in electron optics and detectors, and the correlation of liquid cell microscopy data with probes such as fluorescence, have increased the range of information available from the sample. Because the equipment is not too expensive and works in existing electron microscopes, liquid cell microscopy programs have developed around the world.

### ON OUR WEB SITE

Read the full article at <http://dx.doi.org/10.1126/science.aaa9886>

Advances in electron optics and detectors, and the correlation of liquid cell microscopy data with probes such as fluorescence, have increased the range of information available from the sample. Because the equipment is not too expensive and works in existing electron microscopes, liquid cell microscopy programs have developed around the world.

**OUTLOOK:** Liquid cell electron microscopy is well positioned to explore new frontiers in electrochemistry and catalysis, nanomaterial growth, fluid physics, diffusion, radiation physics, geological and environmental processes involving clays and aerosols, complex biomaterials and polymers, and biological functions in aqueous environments. Continuing improvements in equipment and technique will allow materials and processes to be studied under different stimuli—for example, in extreme temperatures, during gas/liquid mixing, or in magnetic or electric fields. Correlative approaches that combine liquid cell electron microscopy with light microscope or synchrotron data promise a deeper study of chemical, electrochemical, and photochemical reactions; analytical electron microscopy will provide details of composition and chemical bonding in water; high-speed and aberration-corrected imaging extend the scales of the phenomena that can be examined. As liquid cell microscopy becomes more capable and quantitative, it promises the potential to extend into new areas, adopt advanced imaging modes such as holography, and perhaps even solve grand challenge problems such as the structure of the electrochemical double layer or molecular movements during biological processes. ■

The list of author affiliations is available in the full article online.  
\*Corresponding author. E-mail: [fmross@us.ibm.com](mailto:fmross@us.ibm.com)  
Cite this article as F. M. Ross, *Science* 350, aaa9886 (2015). DOI: 10.1126/science.aaa9886

## REVIEW

## ELECTRON MICROSCOPY

# Opportunities and challenges in liquid cell electron microscopy

Frances M. Ross

Transmission electron microscopy offers structural and compositional information with atomic resolution, but its use is restricted to thin, solid samples. Liquid samples, particularly those involving water, have been challenging because of the need to form a thin liquid layer that is stable within the microscope vacuum. Liquid cell electron microscopy is a developing technique that allows us to apply the powerful capabilities of the electron microscope to imaging and analysis of liquid specimens. We describe its impact in materials science and biology. We discuss how its applications have expanded via improvements in equipment and experimental techniques, enabling new capabilities and stimuli for samples in liquids, and offering the potential to solve grand challenge problems.

Transmission electron microscopy (TEM) is a constantly evolving characterization technique that offers atomic-level information on the structure and chemical composition of materials. In materials design, TEM plays a central role by helping to establish structure-property relationships and defect structures. In biology, it provides high-resolution information on biological cells and their components. In physics, time-resolved imaging can probe processes such as phase transformations and directly correlate a material's response to an applied stimulus. TEM is carried out using samples that are stable in the vacuum environment of the microscope and thin enough (e.g., below 100 nm) to give reasonable resolution in images formed by transmitted electrons. However, these requirements have meant that TEM is generally incompatible with liquids, particularly those such as water that have a high vapor pressure.

We describe here a development in TEM that provides the ability to image samples that contain liquids, most importantly water. The difficulty of imaging liquids lies in separating the liquid from the microscope vacuum while achieving a controlled liquid geometry that is thin enough for reasonable image resolution. The solution was understood early on in the development of electron microscopy, but the goal was achieved only when modern microfabrication techniques were used to build thin windows of silicon nitride with a controlled submicrometer separation, between which the liquid could be confined (*1*). This “closed” liquid cell was rapidly developed to include electrodes and flow capabilities and interfaced to the microscope with dedicated sample holders.

The first experiments to make use of these modern liquid cell designs addressed questions

in electrochemical deposition, nanomaterials synthesis, diffusion in liquids, and the structure of biological assemblies. The results, reviewed in (*1*), demonstrated the ability of the liquid cell to probe areas that had traditionally been inaccessible to electron microscopy, and in doing so to achieve useful and unique information. The scope of liquid cell electron microscopy has increased rapidly (*2, 3*). Materials and processes now under study include corrosion, biomolecular structure and dynamics, bubble motion, radiation effects, and biomineralization. Beyond straightforward imaging modes, it is possible to carry out elemental analysis through energy loss or x-ray signals. Advances in electron optics and detectors are now being applied to reduce the electron dose needed and improve the resolution of the images. Finally, correlative techniques, in which electron microscopy signals are combined with other probes such as fluorescence microscopy or synchrotrons, are starting to examine the relationship between function and structural, chemical, and electronic properties. Because processes and structures in liquids are important over such a broad set of scientific and technological areas, the ability to apply the powerful capabilities of TEM to liquid samples promises exciting possibilities for solving grand challenges in materials science, self-assembly, electrochemistry, geology, biology, physics of fluids, and other fields.

## The rapidly developing liquid cell microscopy technique

The early pioneers of transmission electron microscopy were interested in imaging water for both materials science and biological applications and made remarkable progress, given the challenges of observing even solid samples with the microscopes of the time (*4, 5*). Two techniques were developed for getting water into the electron microscope while still maintaining a good enough vacuum to operate the electron source. Both are in use today. One approach (*6*)

is to use differential pumping to enable a high enough pressure at the sample region to allow water droplets to condense. This “open cell” approach became highly successful in environmental scanning electron microscopy (ESEM) (*7, 8*). The TEM community appeared less interested in open cells for water, perhaps because the droplet geometry was not controlled and the maximum pressure was limited. However, liquid droplets in open cells have recently regained popularity in TEM (*9*) for electrochemistry involving low vapor pressure ionic liquids, driven by a need to understand materials transformations during Li-ion battery operation (*10, 11*).

The second approach is closed-cell electron microscopy (*12, 13*) (Fig. 1A). Enclosing water between two electron transparent windows circumvented the limited maximum pressure of the open cell (*5*), but the resolution was reduced by the thick windows used—nitrocellulose (colloidion) was the best material available—and it was difficult to control the window separation. The recent surge of interest in liquid cell microscopy can be attributed to the relative ease of building closed liquid cells using modern microfabrication techniques. The initial liquid cells were homemade, somewhat unreliable, and sealed the liquid hermetically with glue (*14*), but closed liquid cells and the associated TEM equipment are now simpler to use and available commercially.

Almost all microfabricated liquid cells use silicon nitride as the window material. To fabricate windows that are electron transparent yet can withstand the 1-atm pressure difference between the cell interior and the microscope vacuum, a thin film of silicon nitride is deposited onto a silicon wafer and the silicon is etched from the back to form windows with dimensions around 100  $\mu\text{m}$ . The wafer is diced into chips, each containing a window; two such chips are placed face to face, with a spacer material between. This confines the liquid within a thin layer, forming the basic overall design for most closed liquid cells.

To complete the liquid cell (*1*), the chips may be glued, wafer-bonded, or squeezed by clamping in the holder using small o-rings. The spacer may be a solid layer with a channel, or spherical particles. The liquid may be inserted through an entry port etched into one chip (*14–18*) or flowed in through the gap between the chips (*19*). Electrodes can be patterned lithographically inside the closed cell and controlled by an external potentiostat (*14*). In each design, the electrode materials and geometry can be customized for the particular applications (*14, 16, 18, 20–22*). A heating element (*23*) or cooling capability (*24*) can be integrated, and the silicon nitride surfaces can be patterned or chemically modified to enable reactions with species in solution (*25–28*). Careful assembly procedures and cleaning are necessary (*29*). The sample holder is a key part of the liquid cell experiment, and its function extends beyond simply holding the cell securely. It carries the electrical connections between electrode or heater elements and their external controllers. In many designs, it also

IBM T. J. Watson Research Center, 1101 Kitchawan Road, Yorktown Heights, NY 10598, USA.  
E-mail: fmross@us.ibm.com

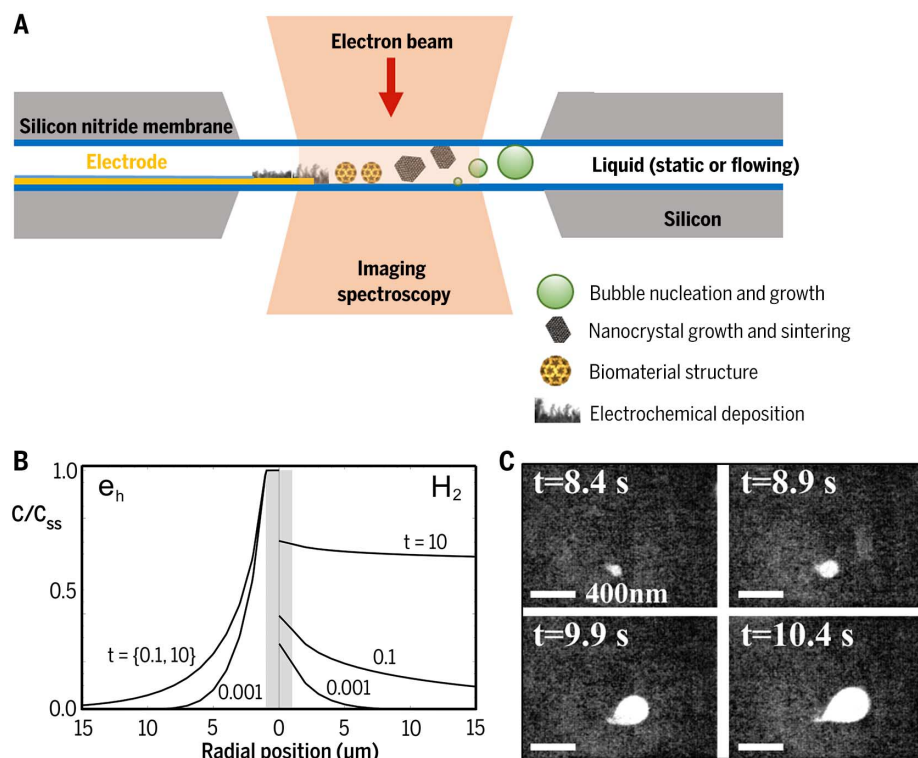


**Fig. 1. The liquid cell microscopy technique.** (A) Schematic diagram of the liquid cell and its application for imaging phenomena in materials science, life science, and physics. The dimensions of the electron beam and the nanoscale objects are exaggerated for clarity. (B) The predicted concentration due to radiolysis,  $C$ , normalized by the steady-state concentration  $C_{SS}$  of  $H_2$  (right) and hydrated electrons  $e_h$  (left) in and around an irradiated area of radius  $1 \mu\text{m}$  (gray stripe) as a function of distance from the beam center at various times in seconds. (C) Image series showing heterogeneous nucleation, growth, detachment, and migration of radiolytic hydrogen bubbles formed during TEM imaging at  $300 \text{ keV}$ , beam current  $< 1 \text{ nA}$  and beam radius  $\sim 2 \mu\text{m}$ . Relative times are shown in seconds. [(B) and (C) adapted with permission from (39) Copyright 2014, American Chemical Society]

provides the vacuum seal by clamping the chips and supplies the liquid through inlet and outlet tubes driven by a syringe pump. Flow enables exciting possibilities of replenishing or changing the solution chemistry while imaging (15, 19, 30).

One of the key ongoing developments in closed liquid cell microscopy is the use of a wider range of TEM capabilities. Initially, liquid cell data was recorded using conventional bright-field TEM or high-angle annular dark-field (HAADF) scanning TEM (STEM) imaging modes. The main decision was whether to record single images, often appropriate for imaging biological structures, or movies of dynamic materials processes, at 30 images per second or whatever the dose rate permits. A wider range of microscopy modes is now common, including dark-field and high-resolution TEM and aberration-corrected imaging (31, 32). Analytical microscopy, both electron energy-loss spectroscopy (EELS) (32, 33) and x-ray energy dispersive spectroscopy (XEDS) (34), is also being applied in liquid cell experiments.

There are two main limitations of liquid cell electron microscopy, image resolution and electron beam effects. Low image resolution is an obvious problem in many liquid cell experiments. Resolution is lost through multiple scattering

of the electrons in both the liquid layer and the window material. The liquid layer is usually thicker than desired, especially toward the center of the window, because the windows bulge outward due to the pressure difference between the interior of the cell and the microscope vacuum. To control the deflection, one can fabricate long thin windows or narrow channels (17); join the windows with posts (16); or use thicker, stiffer membranes with small thin regions for imaging (35). Reducing window separation improves resolution, but we can not decrease the liquid thickness arbitrarily and still expect the liquid cell experiment to be a faithful representation of a “real” phenomenon (9). For example, Brownian motion may differ in ultrathin liquid layers as we discuss below. In electrochemical growth, where diffusion gradients control the kinetics of processes such as deposition, thin liquid layers, may produce results that are different from bulk, making it necessary to calculate the effects of the limited volume (36).

On the other hand, reducing the window thickness improves image quality without affecting the physics of the process under study. The thinnest window material is graphene. High-resolution images can be obtained through liquid droplets

that are placed on a supported graphene membrane, then encapsulated by a second membrane placed on top (37). By using graphene to cover channels in a thicker material, more complex graphene liquid cell designs can be developed (38).

The second major limitation of liquid cell microscopy is the effect of the electron beam. At the energies used in electron microscopy, the beam causes radiolysis of liquids, including water (Fig. 1, B and C). For the conditions appropriate to TEM, calculations show that within seconds, radiolysis products reach equilibrium concentrations in the irradiated region (39, 40) (Fig. 1B). These concentrations depend on dose rate, illuminated area, liquid thickness, and total liquid volume, and can affect the structure or process under study. Radiolytically produced hydrogen gas can exceed its solubility limit and form bubbles (39) (Fig. 1C), which alter the liquid geometry. Hydrogen ions can change the solution pH (40). The highly reactive hydrated (or solvated) electron can drive beam-induced growth of metallic nanoparticles by reducing metallic cations in aqueous salt solutions (41), allowing possibilities for beam writing (39, 42). In combination, radiolytic species can have complex effects (40).

Much work needs to be done to understand electron-beam effects in solutions with multiple dissolved species, as well as in nonaqueous solutions such as ionic liquids. However, existing knowledge of radiation physics can be a guide, and it has already been shown that electron-beam effects can be mitigated with scavenging strategies (43). As microscopists become increasingly familiar with beam effects in liquids, the low-dose techniques developed for biological cryo-electron microscopy are becoming standard, and the benefits of high-sensitivity detectors in reducing the dose required per image are being exploited.

### Liquid cell microscopy for materials science, life science, and beyond

Modern microfabricated liquid cells were first used for electrochemical experiments, recording movies of metal deposition onto electrode surfaces and correlating the images with electrochemical parameters, voltage and current (14, 36, 44, 45). The synthesis of nanoparticles in solution was a second key materials area. The electron beam both triggers growth and allows imaging of the growing and moving nanocrystals (41, 46). In the biological arena, it was quickly realized that, remarkably, few nanometer-size Au labels on biological structures could be resolved even through several micrometers of water (47). Here, we describe highlights of recent results in these areas and in new fields such as biomineralization, the imaging of unlabeled biostructures, bubble dynamics, corrosion, and phase transformations.

### Electrochemistry

The importance of liquid cell microscopy to electrochemistry is that liquid cell experiments enable us to relate the structural and compositional changes that take place to the electrochemical

signature. Other techniques do not probe electrochemical processes with the same combination of temporal and spatial resolution (9, 14, 22). The outcome can be a detailed test of growth mechanisms and information on the phenomena controlling key processes such as corrosion or battery cycling.

#### Understanding growth instabilities

Refining electrochemical growth models is an exciting opportunity for liquid cell microscopy. Initial experiments followed electrodeposition of individual copper nuclei on gold electrodes (14, 36, 44, 45). On further deposition, a polycrystalline film grows over the electrode and then grows beyond it. Understanding the physics governing the morphology of the growth front is essential for controlling the structure and composition of deposited materials. Dynamic observations are helpful because models of solid-liquid interface stability are generally limited to steady-state conditions. Recently, growth instabilities and dendrite formation have been imaged in systems relevant to battery development (18, 20, 40, 48–50). Quantitative measurements of the evolution of the growth front allow us to understand and control growth front stability through additives or pulse deposition (51). Power laws can be obtained for the development of roughness, and local measures such as growth rate at each point on the dendrite are accessible (48). Because diffusion fields play such a key role in electrochemical growth, a key advance has been the demonstration that, under certain circumstances, it is possible to image the distribution of ions in solution through their scattering of transmitted electrons (20).

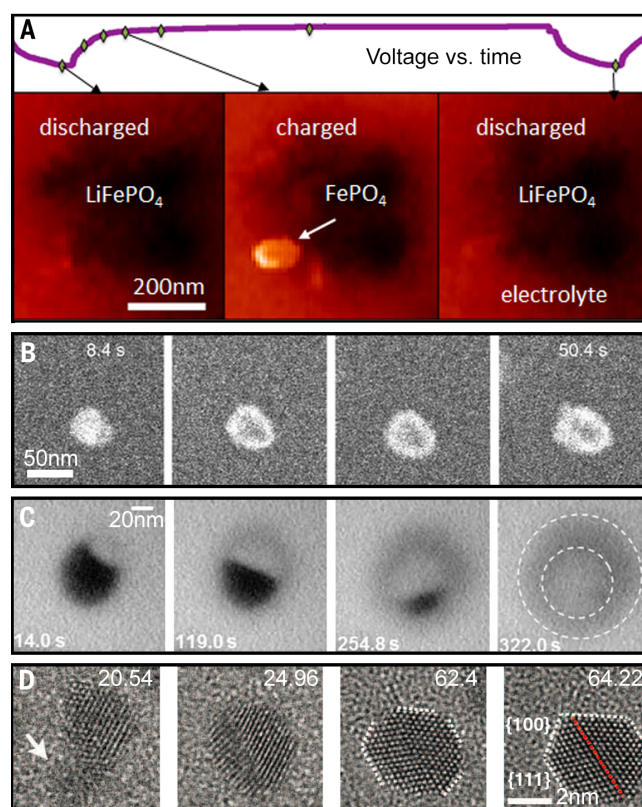
#### Reactions in battery anodes, cathodes, and electrolytes

Interfacial electrochemical reactions control the transport of charge and mass in batteries and energy conversion systems. Liquid cell microscopy enables direct imaging of key phenomena during battery operation. The technique has already produced promising results relevant to Li-ion batteries, for both the key electrode materials and the electrolyte. Adaptation of existing techniques for a wider range of materials—for example, air-sensitive electrolytes—and improved experimental design for quantitative, sensitive (nanoampere) electrochemical measurement (50, 52) are important for these experiments, as is a detailed understanding of the effect of the electron beam on electrochemical measurements.

In electrode materials, dramatic structural and chemical changes take place during cycling. Incorporation of Li changes the volume of some anode materials by hundreds of percent. This volume change can be imaged—for example, in Si in the form of a nanowire attached to a liquid cell electrode (53). The lithiation kinetics in this fully surrounded nanowire differ from those in nanowires that are in contact with electrolyte only at one end (9, 10), illustrating the role of diffusion through the electrolyte. Chemical changes in electrode materials during cycling are also

#### Fig. 2. Liquid processes in nanostructured materials.

(A) The progress of lithium transport across individual particles as voltage is varied during cycling of a  $\text{LiFePO}_4$  particle-based cathode material deposited by slurry printing onto a glassy carbon working electrode. Voltage versus time is shown, and 5-eV energy-filtered maps show delithiated  $\text{FePO}_4$  as bright regions. [Reprinted with permission from (33). Copyright 2014, American Chemical Society] (B) Galvanic replacement of an Ag particle by Pd in 50- $\mu\text{M}$  aqueous  $\text{PdCl}_2$  solution imaged in dark-field STEM at  $6\text{ e}^- \text{ \AA}^{-2} \text{ s}^{-1}$ ; frame time, 8.4 s; electron dose per image,  $52\text{ e}^- \text{ \AA}^{-2}$ . Images are shown at 8.4, 16.8, 25.2, and 50.4 seconds. [Reprinted with permission from (43). Copyright 2014, Macmillan Publishers Ltd.] (C) The formation of a



hollow void in an oxidized Bi nanoparticle via the Kirkendall effect, dominated by nonuniform diffusion of bismuth. Relative times are shown in seconds. [Reprinted with permission from (74). Copyright 2013, American Chemical Society.] (D) High-resolution view in a graphene liquid cell of the sintering of two particles (smaller one arrowed), conversion of the grain boundary into a planar twin boundary, and evolution toward a hexagonal shape consistent with the Wulff construction. [Reprinted with permission of AAAS from (37)]

accessible. The progress of lithium transport across individual particles in a  $\text{LiFePO}_4$  cathode material, resolved using EELS (33), is shown in Fig. 2A.

Battery electrolytes also undergo key changes during cycling: They break down and form a solid electrolyte interphase (SEI) composed of inorganic and organic electrolyte by-products. Understanding the formation of this layer could help improve Li-ion battery safety and cycle life. The structural morphology and evolution of the SEI has recently been observed (54) on highly oriented pyrolytic graphite, cut and joined onto a liquid cell electrode. The use of a three-electrode cell allowed correlation between the onset potential for the electrolyte solvent reduction and the SEI nucleation and growth.

Future battery progress relies on how well one can simulate a “real” battery—in other words, incorporate arbitrary anode and cathode materials in an appropriate geometry, include a reference electrode for quantitative measurements, and surround it all with liquid electrolyte. The development of ways to place nanoparticles, blocks, or strips of materials onto liquid cell electrodes is key (33, 52, 53), as is the availability of electrode materials such as glassy carbon (33). Electron-beam effects can be strong in battery

experiments and may even indicate parameters of electrolyte stability (55).

#### Corrosion and related phenomena

The ability to relate nanoscale microstructural features of corrosion, such as pit formation, with macroscopic, electrochemical parameters is an important motivation for using liquid cell microscopy in understanding corrosion processes. Localized corrosion occurs through breakdown of the protective oxide film on stainless steel and aluminum or titanium alloys, due to aggressive species such as  $\text{Cl}^-$ . Liquid cell movies can show the initiation of pitting when metals such as Cu and Al are exposed to salt solutions, with or without an applied potential (56, 57). This allows measurement of the kinetics and dependence of corrosion morphology on solution concentration. Corrosion mechanisms are often investigated by measuring a Tafel plot—i.e., the current due to dissolution of the material versus the applied voltage. Such data can be obtained using a liquid cell that contains a thin metal film deposited over the window, with a second electrode nearby (57). A wider range of materials can be examined using an approach similar to that described above for batteries: cutting out a lamella of the material of interest and welding it

to the liquid cell electrode (58). If beam effects can be understood (56), the liquid cell technique can provide a unique link between electrochemical parameters and structural change.

### Nanoparticle nucleation, growth, and coalescence

Liquid cell TEM has been used successfully to study colloidal nanoparticle formation, and from the earliest observations it was clear that high spatial and temporal resolution provide opportunities for understanding growth mechanisms, diffusion, and coalescence. The scope of nanoparticle experiments has been augmented by improvements in resolution and by the introduction of heating, which has allowed a greater range of synthesis techniques to be addressed.

#### Growth and etching mechanisms

Metal nanoparticles nucleate and grow when metal ions in solution are reduced by radiolytic hydrated electrons. This beam-induced growth is relevant to real life because irradiation is often used to form particles with a narrow size distribution and without using surfactants. Liquid cell movies allow quantitative measurements of individual particles as they grow, providing a direct view of the mechanisms at work (Fig. 2). Initial experiments (41) showed previously unrecognized growth pathways for Pd nanoparticles, and were able to distinguish the mechanisms of monomer attachment and coalescence. Beam-induced growth has since been observed in other systems (37, 59–61), including multicomponent materials such as core-shell (62) and alloy (63) particles. Measurements as a function of dose rate (64) show the circumstances under which diffusion or attachment control growth. To obtain the highest-quality data from these growth experiments, it is important to improve the time resolution using fast detectors and to track as many particles as possible. Thus, a key advance is data compression and the development of automated video-analysis techniques (67) that can identify simultaneously operating growth mechanisms (64). As well as visualizing the formation of compact nanoparticles, beam-induced growth experiments also show how templates can alter nanoparticle nucleation (66), how beam-induced growth can form extended structures like dendrites (67, 68), and how patterned deposits can be made by rastering the beam (39, 42). Liquid cell microscopy can also image corrosive dissolution of nanoparticles (69, 70). The balance between oxidizing and reducing species produced by radiolysis can lead to situations in which the beam intensity controls particle stability (40, 71).

#### Growth during heating

With the development of heating capabilities, reactions can be driven by temperature rather than the electron beam, to probe other methods of nanoparticle synthesis and structural modification. Examples include hydrothermal precipitation of ZnO, achieved using a thermal reservoir outside the microscope (72), and nucle-

ation of particles by laser heating (73). Complex phenomena can be visualized, such as Kirkendall voids formed by oxidizing Bi nanoparticles at elevated temperature (74) (Fig. 2C) and oscillatory growth of Bi nanoparticles exchanging material on heating (75).

#### Factors determining particle shape

As liquid cell resolution improves through the use of aberration correction and high-speed imaging (31) or graphene windows (37), it becomes possible to determine the nature and evolution of nanoparticle facets (31, 60) (Fig. 2D). Such experiments show how surfactants control which facets form (60) and how they may alter facet growth rates, even breaking the surface energy minimization rule so that growth does not follow the Wulff plot (31).

#### Dynamics of coalescence

As particles coalesce in solution into larger assemblies, liquid cell microscopy provides a remarkable view of the processes at work. Observing the dynamic motions and rotations of particles as they approach provides direct information on interparticle forces (59, 76, 77). Coalescence appears to take place on preferred planes (37). Particles may approach multiple times until they rotate into registry and snap together (77). Defect formation during coalescence can be imaged (Fig. 2D), as can structural rearrangements after coalescence. When multiple particles assemble, superlattices or diffusion-limited aggregates may form, and aggregation parameters (62, 78) and orientational order parameters of superlattices (79) can be measured. A common theme, of importance to synthesis and biomineralization, is the rich variety of growth pathways possible; it becomes clear that the final shape of a particle assembly alone provides only limited information on its formation mechanism.

#### Phase transformations in liquids

Electron microscopy has a distinguished history in exploring phase transformations and reactions in solids (2). The recent development of heating and cooling in liquid cells allows temperature, the key thermodynamic parameter, to be controlled, and therefore a range of transformations to be accessed.

Heating water nucleates bubbles, and their nucleation, growth, and stability can be measured and compared with thermodynamic models (23). Localized heating is achieved via Joule strips made of Pt lines, and the temperature gradients can in principle be modeled. Heating via an external reservoir results in more uniform temperature; laser heating (73), through a fiberoptic or port on the column, enables rapid temperature changes. Given the variety of heating methods, experiments can be optimized for the phenomenon under study, suggesting rich future possibilities.

Cooling allows ice to form from liquid water (provided beam-induced heating is minimized). Solidification of saline solutions containing Au nanoparticles (24)—using a cold finger in contact with the liquid cell—has provided insights into

the competition between hexagonal and cubic ice nucleation and growth as a function of temperature, as well as particle rejection and occlusion as the ice advances (Fig. 3A). These types of experiments yield information that is complementary to what can be obtained from cold-stage experiments in ESEM and TEM in which water (80) (Fig. 3B) or ice (81) condense from vapor.

#### The physics of fluids at the nanoscale

Fluid physics is another area where our understanding can benefit from observations at nanometer length scales and especially at improved temporal resolution. Liquid cell microscopy can show how water moves at small length scales, how nanoscale bubbles move in water, and how nanoscale objects move within thin water films.

It is easy (often unavoidable) to form bubbles by radiolysis of the water in a liquid cell (39, 40, 82). As a large bubble forms, water recedes across the silicon nitride windows and leaves a thin wetting layer. Voids form in this layer, and their growth or shrinkage depends on size (83). Ultrathin droplets form, as do more complex structures that are thought to be caused by droplet charging (84). The droplets move with a stick-slip appearance, demonstrating the importance of interfacial interactions to nanoscale fluidity (84). Small bubbles in comparably thick liquid films drift up thickness gradients, and this motion can be modeled by considering the effects of trijunction forces (85).

The nucleation and motion of small droplets and the movement of bubbles in confined volumes is important in a range of fields, including catalysis, cavitation and lubrication, degassing of fluids, and boiling. Recent experiments have therefore examined liquid dynamics in other constrained geometries. Cylinders can be made from carbon nanotubes (86) or by using a graphene stack that curls into scrolls around the liquid (87). This provides the opportunity to observe bubble dynamics, condensation, and other processes in restricted volumes and offers the useful option of imaging parallel to the liquid/solid interface (Fig. 3B).

Particle motion in response to liquid motion (46) is readily observed from liquid cell experiments. Brownian motion can also be quantified. Nanoparticles in thin layers move much more slowly than expected for a bulk liquid (78, 88–90); the discrepancy can be 7 to 9 orders of magnitude. Such highly damped diffusive movement is helpful for recording images, but it is unexpected based on calculations of water in pores (91). If this damping arises from interactions between particle and substrate, it may be worth exploring other window materials (37).

#### Environmental and biological mineralization

The mechanisms that control key biological and environmental processes, such as mineral formation, are not well understood, partly due to the difficulty of making observations with appropriate resolution during growth. Liquid cell microscopy provides information on aggregation

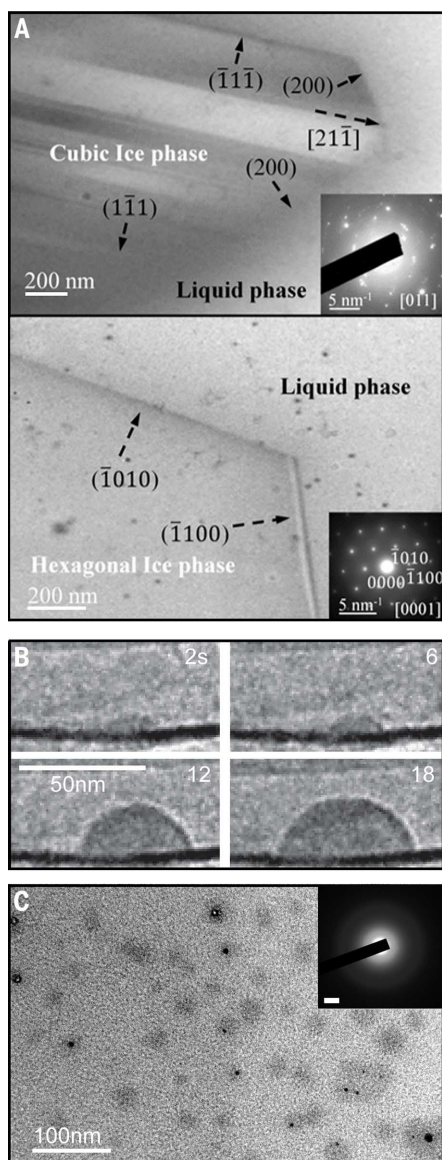


**Fig. 3. Phase transformations.** (A) Ice crystallizing from saline solution at 245 and 260 K (upper and lower images) showing the competition between different solid phases, identified by diffraction. [From (24). Copyright Microscopy Society of America, 2014] (B) A nanodroplet within a graphene nanochannel scroll imaged after the times shown. The hemispherical cap-shaped droplet condenses and grows on the wall. [Reproduced from (87) with permission from The Royal Society of Chemistry] (C) Amorphous CaCO<sub>3</sub> nucleation (dark points) within an organic matrix containing Ca-polystyrene sulphonate globules (larger patches). Nucleation sites are within the organic matrix, with an amorphous structure seen in diffraction data (inset). [Reprinted with permission from (95), Macmillan Publishers Ltd, copyright 2015]

processes, an example being the geological material iron oxyhydroxide (77). Key biomineralization questions can be examined, such as the effect of organic materials on nucleation pathways

(92–95). Figure 3C (95) illustrates how, by binding calcium, organic additives bias calcium carbonate nucleation toward the amorphous phase rather than a crystalline phase. These experiments illustrate an innovative design in which CO<sub>2</sub> was diffused through one inlet of a dual-inlet liquid cell holder into a calcium-bearing solution to gradually raise supersaturation. This type of approach may be useful in other materials systems.

Biomineralization can also be investigated in whole (single-cell) organisms. Magnetotactic bacteria construct magnetosomes, chains of magnetite crystals. Correlative liquid cell STEM and fluorescence microscopy (Fig. 4A) explore magnetosome structure in the natural cellular environment (96). These images are static, but dynamic information could in principle be obtained if the dose can be kept low. The success of liquid cell microscopy in imaging systems containing both soft macromolecular matrices and hard mineral constituents suggests that the technique will be applicable to many key biomineralization processes.

### Liquid cell microscopy for life science

Microscopy has been a driver for discovery in life science. Fluorescence microscopy can image specific proteins at up to 10-nm resolution if superresolution techniques are used and can image protein dynamics and interactions in fixed or living cells. Electron microscopy can offer higher resolution on material that is encased in amorphous ice at cryogenic temperature or on dried or embedded material at room temperature. Correlative light and electron microscopy uses the strengths of both techniques to provide detailed structural and functional information. Unfortunately, the resolution benefits of electron microscopy are associated with the challenge of preserving the material during conventional sample preparation. Dehydration or freezing changes the structure and, of course, removes the possibility of making dynamic observations or imaging living cells. The pioneering demonstrations that labeled biological structures can be resolved through micrometers of water using STEM (47, 97), and that biological processes can be stimulated in situ by injecting nutrients (30), showed that liquid cell microscopy can provide high-resolution information while circumventing some of the sample preparation issues. Liquid cell TEM is therefore positioned well as a complement to conventional light and electron microscopy methods to address the complexity of biological materials.

### Whole cells and live cells

The ability to image nanoparticle labels through thick liquid enables the study of cell structure and function. Cells can be grown on an electron transparent membrane chip, incubated for different times or under varied conditions with labels that tag specific proteins or are taken up by the cells, and then enclosed by adding the top chip. Liquid cell microscopy can visualize the tagged structures or measure particle uptake

(47, 48, 98) (Fig. 4B). Correlative experiments involving fluorescence microscopy (99) provide additional information on cell structure and viability. Correlative light and liquid cell microscopy has been used to measure the spatial distribution of a growth factor that is expressed in tumor cells (100), finding a nonuniform distribution over the cell membrane that may be relevant to metastasis and drug response. An important step forward for such studies is the statistical information obtained by measuring relatively large numbers of cells in a short time, enabled through optimization of experimental procedures (101). The interactions of cell edges with nanoparticles can also be imaged (102). Studies of this type may have relevance to safety and dose evaluation for nanoparticle-based drug-delivery vehicles.

If the enclosure has suitable size and surface condition, and if nutrients are supplied, unfixed cultured cells can be kept alive in a liquid cell chamber at room temperature with liquid flow for several hours (97, 103). But is it possible for cells to remain alive while images are recorded? Although unfixed cells can be imaged, it appears that they are not viable after even one image is recorded (103), even with liquid flow to provide nutrients and perhaps remove radiolysis products and heat during imaging. The dose delivered in one image is typically above the lethal dose. There is much ongoing interest in establishing whether tolerable doses exist for in vivo liquid cell microscopy (96, 103); it may be possible to study certain biochemical processes, as it appears that the speed of cell death depends on the region of the cell that is imaged.

### Tracking motion in labeled biological systems

It is possible to visualize certain biological functions by tracking the movements of the labels attached to them. An interesting example (30) is the movement of the myosin head in response to adenosine triphosphate (ATP). These experiments involve synthetic myosin muscle filaments, labeled with Au particles and placed on one surface of a large liquid cell chamber filled with saturated air. ATP is injected through a capillary, diffusing to the sample through the surface liquid layer and stimulating a several-nanometer filament movement. Labels can also be attached to smaller biomolecules such as DNA. The motion of pairs of gold nanoparticles tethered by a single piece of double-stranded DNA gives information on DNA configuration under the electron beam (104).

### Imaging unlabeled biostructures, soft materials, and dynamical phenomena

Under favorable conditions, biomolecules and macromolecular assemblies can be imaged without the use of nanoparticle labels and at relatively low dose. Favorable imaging conditions include the lowest possible liquid and window thickness and a strategy for minimizing motion blur during image acquisition. One approach is to closely encase the material with graphene,

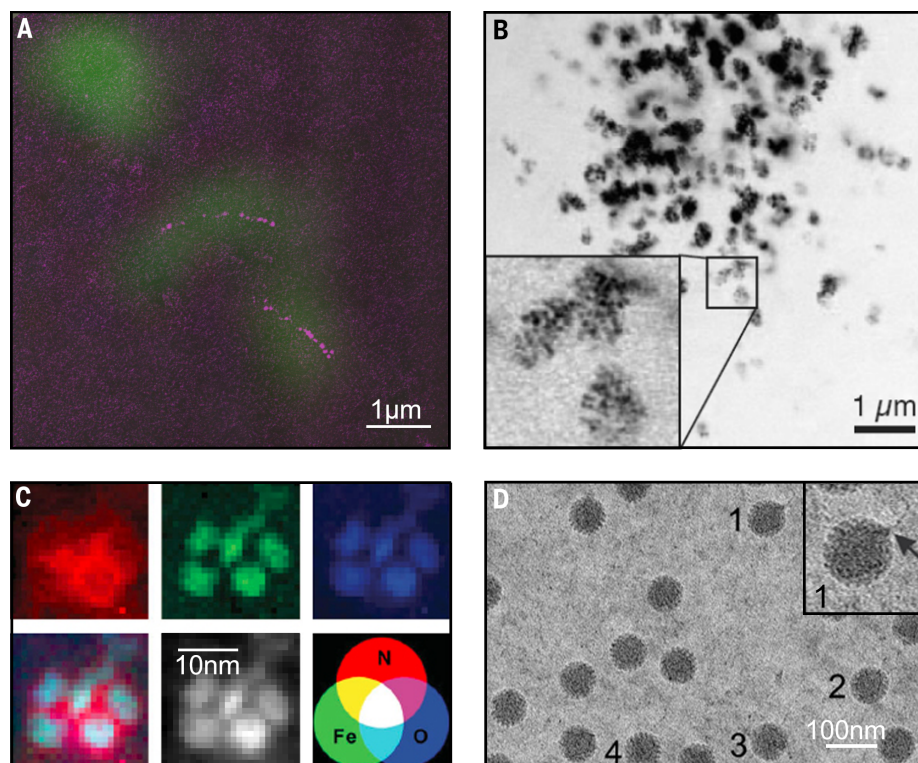


**Fig. 4. Biological structures and processes.** (A) Superimposed fluorescence and STEM images of two viable cells of *Magnetospirillum magneticum*. The magnetosome chains appear in purple. Scale bar, 1  $\mu\text{m}$ . [From (96). Reprinted by permission from Macmillan Publishers Ltd., copyright 2014] (B) Live whole COS7 cells during nanoparticle take-up, imaged 24 hours after their incubation with serum-protein coated 30-nm Au nanoparticles. The particles were found in a dense, three-dimensional cluster of vesicles. The inset represents a processed image of the indicated region, with individual particles visible within the vesicles. [Reprinted from (97)] (C) Compositional maps for N, Fe, and O obtained for ferritin molecules in water sandwiched between graphene sheets with 1-nm resolution. A composite map (see color chart) and a HAADF image are also shown. The raw data are filtered to improve signal to noise. The protein shell of ferritin is clearly resolved and the iron valence identified as 3+. [Reprinted with permission from (107)] (D) Double-layered particles, the structures into which rotavirus transforms on invading a host cell, imaged while actively transcribing mRNA. The particles are tethered to SiN microchips, and ATP was added to enable transcription. Single-stranded mRNA is seen around several viral capsids (1 to 4 and inset). [From (27). Copyright Royal Society of Chemistry, 2015]

minimizing the membrane thickness and the volume of surrounding liquid (105, 106). Another approach is to use patterned silicon nitride substrates with microwells that control the liquid thickness (25, 26) and additionally to tether biostructures by functionalizing the substrate (26–28).

Such improvements can result in high-quality imaging of biomaterials and soft materials in the liquid state. High-contrast materials, such as the magnetosomes mentioned above (96), ferritin molecules (107) (Fig. 4C), and micelles containing heavy metals (108), are readily imaged to show their overall structure. Analytical techniques can provide composition and bonding, as has been shown for ferritin using EELS (107), and dynamics can be studied, as has been shown for Pt-containing micelles (108). However, even low-atomic-number materials are visible using liquid cell microscopy. Liposomes and polymers have been imaged (109, 110) to provide

shape and size in water, a useful comparison with cryoelectron microscopy results. In addition, more complex biostructures can be imaged. For example, the acrosomal process, a membrane that extends from sperm heads, has an appearance in the liquid cell that is consistent with that in cryoelectron microscopy (28). Protein crystals have been imaged at 2.7-nm resolution with a cumulative electron dose of 3500 electrons per  $\text{nm}^2$  (28). The combination of TEM and fluorescence microscopy has been used to determine the spatial distributions and interactions of subcellular organelles, such as the cytoskeleton and its contact with adjacent cells (111). Finally, Fig. 4C shows a viral pathogen imaged at  $\sim 3$ -nm resolution in the process of transcribing RNA (27). With image processing, these data are sensitive to rearrangements in the internal structure of the virus during RNA synthesis. Tests for viability are important in evaluating experiments involving dynamic biochemical processes (27).

Because liquid cell electron microscopy is a new technique, it is important to validate all of its results by comparison with cryoelectron microscopy and to establish radiation damage criteria. However, these recent advances provide encouragement that liquid cell microscopy might complement cryoelectron microscopy, fluorescence, and diffraction techniques in providing static and dynamic imaging of biological systems in water, fulfilling the critical need to develop real-time, high-resolution imaging tools for life sciences.

## Future prospects

### Geological materials such as clays

The hydration of clay minerals is important for soil properties, in developing building materials, and in mining activities. Microscopy of clay minerals in a controlled environment that includes liquid water should provide new information on the pathways by which the key structural transformations occur. Early research in this area (5, 112) on the hydration of Portland cement was hampered by the lack of a reliable method for handling water in situ. Modern liquid cells have a greater chance of producing quantitative results in, for example, imaging the behavior of the swelling clays (montmorillonites or bentonites) in fluids of different compositions. Hydration behavior in confined volumes is well suited for liquid cell experiments and could provide information relevant to oil sand extraction. Many minerals with hydrated and anhydrous varieties have commercial value, and others cause problems when they change state. There appears to be no shortage of interesting questions in this area.

### Extreme temperature and pressure geological processes

Conventional liquid cells can withstand pressures of only a few atmospheres (20). How far we can push this upper pressure limit depends on the mechanical properties of the windows. Inorganic fluids confined in liquid cells at high pressures can perhaps provide nanoscale insights into geological processes such as hydrothermal reactions relevant to crystal growth, nanostructure synthesis, fuel production, or volcanic activity. The nature of many hydrothermal chemical reactions is difficult to assess, and nanoscale in situ observations could provide new insights. At low temperatures, the structure and stability of methane clathrates could be a useful field of study.

### Atmospheric aerosols

Environmental TEM provides valuable information for understanding the behavior and properties of atmospheric particles (113). However, its use is limited at high relative humidities, in particular the extreme of complete saturation. The full ability to control the water environment is relevant to cloud formation, where saturation and supersaturation values are high. We could imagine, for example, subjecting various types of common atmospheric particles to water and liquids with different salinities and

observe phase changes during cooling at controlled rates.

### Biomaterials

The recent results described above suggest further applications in a wider range of mineral systems and environments, including those involving organic components. Multiple mineral phases and reaction pathways are a common characteristic, and comparing different systems would allow an understanding of the principles that determine which pathway will be followed and how nucleation can be directed with control over phase, orientation, and location.

### Physics of fluids

A grand challenge for understanding interfacial fluids has been the difficulty of imaging liquid/solid interfaces with good time and space resolution (114). Given the improvements in liquid cell microscopy resolution and detector sensitivity, we anticipate that studies over the next few years should illuminate features of the liquid/solid interface such as ordering, the hydration layer, and the double layer, and provide direct observations of phase transitions. Diffusion through liquids is important in catalysis, battery operation, biomaterials, and tribology. With the development of low-temperature imaging, it could be exciting to examine liquids such as nitrogen or even helium, and solvents such as liquid ammonia.

### Electrochemistry in more complex systems

There has been little study of materials other than metals, of codeposition and electroless deposition, or of temperature-dependent electrochemistry. Take, for example, the electrochemically deposited polymers: Polypyrrole is an extensively studied conducting polymer, whose most efficient synthesis method is electropolymerization (115). Temperature-dependent electrochemistry, including low-temperature Li-ion battery function, is a critical area. It is possible that molten salt electrochemical reactions relevant to Al refining or the process of stress corrosion cracking could be performed in extreme environments of water and high temperature and pressure.

### The electrochemical double layer

A grand challenge for microscopy is to image directly the electrochemical double layer and measure its behavior during electrochemical processes. Its length scale of a few nanometers makes this difficult, but experiments may involve combinations of holography and liquid cell microscopy to probe the double layer at an atomically flat electrode surface.

### Magnetic materials

The holography/liquid cell combination provides other fascinating opportunities. One can imagine in situ observation during liquid phase deposition of magnetic materials, simultaneously measuring their developing microstructure and magnetic fields. Magnetic thin films such as the NiFe layers used in magnetic read heads

are formed by electroless deposition at moderate temperatures, and understanding film evolution could potentially improve our control of nucleation and domain development. Other areas of application include the interactions of magnetic particles in liquids and the behavior of the surfactant-coated particles within ferrofluids while being magnetized.

### Catalysis

Electron microscopy has provided detailed insights into catalysis from gases (116, 117) but is relatively less explored for reactions that form liquids (118) or that are catalyzed by liquids (119). As liquid geometry and flow become better controlled, we can now envisage liquid cell microscopy of catalyst reactions involving water. Water splitting can be achieved by catalysts driven electrochemically or with light fed through a fiber optic, as already demonstrated in gas-phase catalysis (117), and this will likely be a key application area for liquid cell microscopy.

### High-speed phenomena

The ability to record liquid cell data at high frame rates expands the range of phenomena that can be addressed and also improves image resolution by reducing motion-induced blur. For even faster processes, though, the technique of dynamic TEM (DTEM) can be adapted for the liquid cell (82). A laser hits the sample, supplying heat or optical stimulation, and also triggers a pulse of electrons (delayed by a specified time) that form an image. The time resolution, determined by the length of the pulse, is 1  $\mu$ s to 1 ns. Microanalysis is possible via energy-filtered TEM through an in-column filter. So far, laser-induced nucleation and growth has been examined at  $\sim$ 10-nm spatial resolution (73), and DTEM is likely to have broad application for rapid liquid-mediated reactions.

### Imaging whole biological cells

Imaging cells in their native liquid state is already an exciting prospect, offering the possibility of high-resolution information without freezing or drying. It is not yet clear whether live cells can ever be imaged. We need a better understanding of dose effects, through correlative experiments that determine the extent to which biological functions are preserved during imaging. Indeed, irradiation effects on cells (with taken-up nanoparticles, for example) could provide insights into cancer therapies. Because various parts of a cell show different dose tolerances, it may be useful to develop systems with optimized liquid geometry to allow dose-tolerant regions to be imaged with good resolution and minimized dose. To distinguish different components within a cell, the use of mixtures of labels could be explored in liquid cell TEM, as is done for fluorescence microscopy.

### The structures of biomaterials and proteins

The current progress in liquid cell microscopy of unlabeled biomaterials, combined with greater use of techniques already developed for cryo-EM—such as low-dose imaging, dose fractionation

techniques, and image analysis techniques—suggests that in the future the technique could provide insights into the structure of materials such as block copolymers, protein domains, macromolecule-mediated nanoparticle assembly, and even food materials. The liquid environment may provide a benefit, compared with cryoelectron microscopy, if it can be shown to help move away radiolysis products while preserving structure. In addition, temperature control will prove useful in understanding interactions and processes in these types of materials.

### Imaging biological dynamics

Movies of processes such as the dynamics of large proteins, changes in membrane geometry, or the assembly of microfilaments would provide fundamental and practical insights. Prospects for real-time imaging ultimately come down to the dose required per image. Increasing the material contrast reduces the dose required; achieving higher contrast (without using labels or defocus techniques) may require exploring the use of phase plates (120) or electron holography (121). Temperature-dependent imaging of biological structures and processes could allow optimum temperatures to be chosen for measurements of dynamics and exploration of biological processes under extreme environments. The processes may be triggered by introducing chemicals into the solution flow [as demonstrated in (30)] or by laser pumping (as in DTEM) by heating or direct light stimulation. Because biological systems also respond to electromagnetic fields, the use of externally applied fields, with results measured using holography, could be potentially transformative, if issues of dose and the holographic reference beam could be resolved. This could possibly produce charge maps of proteins and show the self-assembly and folding of proteins or the field-induced interactions between individual biomolecules and binding sites. Although some of the above speculations appear far from reality, the recent pace of progress encourages us to expect a strong impact of liquid cell microscopy for understanding biological structures and processes.

The examples described above, covering both current research and future ideas, suggest that liquid cell electron microscopy is well positioned to explore new frontiers in nanomaterial growth, fluid physics, radiation physics, corrosion and electrochemical processes, geological and environmental processes, and biomaterial structure and function. Based on continuing improvements in equipment and experimental capabilities, we anticipate that observations made using liquid cell microscopy can address key materials challenges and provide an exciting view of liquid-phase materials and processes.

### REFERENCES AND NOTES

1. N. de Jonge, F. M. Ross, Electron microscopy of specimens in liquid. *Nat. Nanotechnol.* **6**, 695–704 (2011). doi: [10.1038/nnano.2011.161](https://doi.org/10.1038/nnano.2011.161); pmid: 22020120
2. R. Sinclair, In situ high-resolution transmission electron microscopy of material reactions. *Mater. Res. Soc. Bull.* **38**, 1065–1071 (2013). doi: [10.1557/mrs.2013.285](https://doi.org/10.1557/mrs.2013.285)

3. H.-G. Liao, K. Niu, H. Zheng, Observation of growth of metal nanoparticles. *Chem. Commun.* **49**, 11720–11727 (2013). doi: [10.1039/c3cc47473a](https://doi.org/10.1039/c3cc47473a); pmid: [2421213](https://pubmed.ncbi.nlm.nih.gov/2421213/)
4. D. F. Parsons, Structure of wet specimens in electron microscopy. Improved environmental chambers make it possible to examine wet specimens easily. *Science* **186**, 407–414 (1974). doi: [10.1126/science.186.4162.407](https://doi.org/10.1126/science.186.4162.407); pmid: [4213401](https://pubmed.ncbi.nlm.nih.gov/4213401/)
5. E. P. Butler, K. F. Hale, *Dynamic Experiments in the Electron Microscope* (North-Holland, 1981), Chapter 6.
6. E. Ruska, Beitrag zur uebermikroskopischen Abbildungen bei hoeheren Drucken. *Kolloid Z.* **100**, 212–219 (1942). doi: [10.1007/BF01519549](https://doi.org/10.1007/BF01519549)
7. G. D. Danilatos, Review and outline of environmental SEM at present. *J. Microsc.* **162**, 391–402 (1991). doi: [10.1111/j.1365-2818.1991.tb03149.x](https://doi.org/10.1111/j.1365-2818.1991.tb03149.x)
8. D. Stokes, *Principles and Practice of Variable Pressure/Environmental Scanning Electron Microscopy (VP-ESEM)* (Wiley, 2008).
9. C.-M. Wang, H.-G. Liao, F. M. Ross, Observation of materials processes in liquids by electron microscopy. *MRS Bull.* **40**, 46–52 (2015). doi: [10.1557/mrs.2014.283](https://doi.org/10.1557/mrs.2014.283)
10. J. Y. Huang *et al.*, In situ observation of the electrochemical lithiation of a single SnO<sub>2</sub> nanowire electrode. *Science* **330**, 1515–1520 (2010). doi: [10.1126/science.1195628](https://doi.org/10.1126/science.1195628); pmid: [21148385](https://pubmed.ncbi.nlm.nih.gov/21148385/)
11. C. M. Wang *et al.*, In situ transmission electron microscopy and spectroscopy studies of interfaces in Li ion batteries: Challenges and opportunities. *J. Mater. Res.* **25**, 1541–1547 (2010). doi: [10.1557/JMR.2010.0198](https://doi.org/10.1557/JMR.2010.0198)
12. I. M. Abrams, J. W. McBain, A closed cell for electron microscopy. *Science* **100**, 273–274 (1944). doi: [10.1126/science.100.2595.273](https://doi.org/10.1126/science.100.2595.273); pmid: [17746136](https://pubmed.ncbi.nlm.nih.gov/17746136/)
13. D. D. Double, A. Hellawell, S. J. Perry, The hydration of Portland cement. *Proc. R. Soc. London Ser. A* **359**, 435–451 (1978). doi: [10.1098/rspa.1978.0050](https://doi.org/10.1098/rspa.1978.0050)
14. M. J. Williamson, R. M. Tromp, P. M. Vereecken, R. Hull, F. M. Ross, Dynamic microscopy of nanoscale cluster growth at the solid-liquid interface. *Nat. Mater.* **2**, 532–536 (2003). doi: [10.1038/nmat944](https://doi.org/10.1038/nmat944); pmid: [12872162](https://pubmed.ncbi.nlm.nih.gov/12872162/)
15. C. Mueller, M. Harb, J. R. Dwyer, R. J. D. Miller, Nanofluidic cells with controlled pathlength and liquid flow for rapid, high-resolution in situ imaging with electrons. *J. Phys. Chem. Lett.* **4**, 2339–2347 (2013). doi: [10.1021/jz401067k](https://doi.org/10.1021/jz401067k)
16. J. M. Grogan, H. H. Bau, The nanoaquarium: A platform for in situ transmission electron microscopy in liquid media. *J. Microelectromech. Syst.* **19**, 885–894 (2010). doi: [10.1109/JMEMS.2010.2051321](https://doi.org/10.1109/JMEMS.2010.2051321)
17. E. Jensen, A. Burrows, K. Mølhave, Monolithic chip system with a microfluidic channel for in situ electron microscopy of liquids. *Microsc. Microanal.* **20**, 445–451 (2014). doi: [10.1017/S1431927614000300](https://doi.org/10.1017/S1431927614000300); pmid: [24717178](https://pubmed.ncbi.nlm.nih.gov/24717178/)
18. A. J. Leenheer, J. P. Sullivan, M. J. Shaw, C. T. Harris, A sealed liquid cell for in situ transmission electron microscopy of controlled electrochemical processes. *J. Microelectromech. Syst.* **24**, 1061–1068 (2015). doi: [10.1109/JMEMS.2014.2380771](https://doi.org/10.1109/JMEMS.2014.2380771)
19. E. A. Ring, N. de Jonge, Microfluidic system for transmission electron microscopy. *Microsc. Microanal.* **16**, 622–629 (2010). doi: [10.1017/S1431927610093669](https://doi.org/10.1017/S1431927610093669); pmid: [20804635](https://pubmed.ncbi.nlm.nih.gov/20804635/)
20. E. R. White *et al.*, In situ transmission electron microscopy of lead dendrites and lead ions in aqueous solution. *ACS Nano* **6**, 6308–6317 (2012). doi: [10.1021/nm3017469](https://doi.org/10.1021/nm3017469); pmid: [22702348](https://pubmed.ncbi.nlm.nih.gov/22702348/)
21. B. L. Mehdi *et al.*, In-situ electrochemical transmission electron microscopy for battery research. *Microsc. Microanal.* **20**, 484–492 (2014). doi: [10.1017/S1431927614000488](https://doi.org/10.1017/S1431927614000488); pmid: [24755142](https://pubmed.ncbi.nlm.nih.gov/24755142/)
22. R. R. Unocic *et al.*, Quantitative electrochemical measurements using in situ ec-S/TEM devices. *Microsc. Microanal.* **20**, 452–461 (2014). doi: [10.1017/S1431927614000166](https://doi.org/10.1017/S1431927614000166); pmid: [24618013](https://pubmed.ncbi.nlm.nih.gov/24618013/)
23. E. R. White, M. Mecklenburg, S. B. Singer, S. Aloni, B. C. Regan, Imaging nanobubbles in water with scanning transmission electron microscopy. *Appl. Phys. Express* **4**, 055201 (2011). doi: [10.1143/APEX.4.055201](https://doi.org/10.1143/APEX.4.055201)
24. K. Tai, Y. Liu, S. J. Dillon, In situ cryogenic transmission electron microscopy for characterizing the evolution of solidifying water ice in colloidal systems. *Microsc. Microanal.* **20**, 330–337 (2014). doi: [10.1017/S1431927613014128](https://doi.org/10.1017/S1431927613014128); pmid: [24548432](https://pubmed.ncbi.nlm.nih.gov/24548432/)
25. K. Degen, M. Dukes, J. R. Tanner, D. F. Kelly, The development of affinity capture devices—a nanoscale purification platform for biological in situ transmission electron microscopy. *RSC Adv.* **2**, 2408–2412 (2012). doi: [10.1039/c2ra01163h](https://doi.org/10.1039/c2ra01163h)
26. M. J. Dukes *et al.*, Improved microchip design and application for in situ transmission electron microscopy of macromolecules. *Microsc. Microanal.* **20**, 338–345 (2014). doi: [10.1017/S1431927613013858](https://doi.org/10.1017/S1431927613013858); pmid: [24331164](https://pubmed.ncbi.nlm.nih.gov/24331164/)
27. A. C. Varano *et al.*, Visualizing virus particle mobility in liquid at the nanoscale. *Chem. Commun.* **51**, 16176 (2015). doi: [10.1039/c5cc05744b](https://doi.org/10.1039/c5cc05744b)
28. U. M. Mirsaidov, H. Zheng, Y. Casana, P. Matsudaira, Imaging protein structure in water at 2.7 nm resolution by transmission electron microscopy. *Biophys. J.* **102**, L15–L17 (2012). doi: [10.1016/j.bpj.2012.01.009](https://doi.org/10.1016/j.bpj.2012.01.009); pmid: [22385868](https://pubmed.ncbi.nlm.nih.gov/22385868/)
29. D. B. Peckys, N. de Jonge, Studying the stoichiometry of epidermal growth factor receptor in intact cells using correlative microscopy. *J. Vis. Exp.* **103**, e53186 (2015). doi: [10.3791/53186](https://doi.org/10.3791/53186)
30. H. Sugii *et al.*, Direct demonstration of the cross-bridge recovery stroke in muscle thick filaments in aqueous solution by using the hydration chamber. *Proc. Natl. Acad. Sci. U.S.A.* **105**, 17396–17401 (2008). doi: [10.1073/pnas.0809581105](https://doi.org/10.1073/pnas.0809581105); pmid: [18987316](https://pubmed.ncbi.nlm.nih.gov/18987316/)
31. H. G. Liao *et al.*, Facet development during platinum nanocube growth. *Science* **345**, 916–919 (2014). doi: [10.1126/science.1253149](https://doi.org/10.1126/science.1253149); pmid: [25146287](https://pubmed.ncbi.nlm.nih.gov/25146287/)
32. K. L. Jungjohann, J. E. Evans, J. A. Aguiar, I. Arslan, N. D. Browning, Atomic-scale imaging and spectroscopy for in situ liquid scanning transmission electron microscopy. *Microsc. Microanal.* **18**, 621–627 (2012). doi: [10.1017/S1431927612000104](https://doi.org/10.1017/S1431927612000104); pmid: [22640296](https://pubmed.ncbi.nlm.nih.gov/22640296/)
33. M. E. Holtz *et al.*, Nanoscale imaging of lithium ion distribution during in situ operation of battery electrode and electrolyte. *Nano Lett.* **14**, 1453–1459 (2014). doi: [10.1021/nl404577c](https://doi.org/10.1021/nl404577c); pmid: [24548177](https://pubmed.ncbi.nlm.nih.gov/24548177/)
34. E. A. Lewis *et al.*, Real-time imaging and local elemental analysis of nanostructures in liquids. *Chem. Commun.* **50**, 10019–10022 (2014). doi: [10.1039/C4CC02743D](https://doi.org/10.1039/C4CC02743D); pmid: [24831648](https://pubmed.ncbi.nlm.nih.gov/24831648/)
35. J. F. Creemer *et al.*, Atomic-scale electron microscopy at ambient pressure. *Ultramicroscopy* **108**, 993–998 (2008). doi: [10.1016/j.ultramic.2008.04.014](https://doi.org/10.1016/j.ultramic.2008.04.014); pmid: [18556124](https://pubmed.ncbi.nlm.nih.gov/18556124/)
36. A. Radisic, P. M. Vereecken, J. B. Hannon, P. C. Seanson, F. M. Ross, Quantifying electrochemical nucleation and growth of nanoscale clusters using real-time kinetic data. *Nano Lett.* **6**, 238–242 (2006). doi: [10.1021/nl052175j](https://doi.org/10.1021/nl052175j); pmid: [16464042](https://pubmed.ncbi.nlm.nih.gov/16464042/)
37. J. M. Yuk *et al.*, High-resolution EM of colloidal nanocrystal growth using graphene liquid cells. *Science* **336**, 61–64 (2012). doi: [10.1126/science.1217654](https://doi.org/10.1126/science.1217654); pmid: [22491849](https://pubmed.ncbi.nlm.nih.gov/22491849/)
38. V. P. Adiga, G. D. Dunn, A. P. Alivisatos, A. Zettl, Electrically integrated graphene on silicon nitride liquid flow cells for high resolution electron microscopy, U.S. Patent Application Ser. No. 14/817,551. <http://ipo.lbl.gov/ibn2014-129/>.
39. J. M. Grogan, N. M. Schneider, F. M. Ross, H. H. Bau, Bubble and pattern formation in liquid induced by an electron beam. *Nano Lett.* **14**, 359–364 (2014). doi: [10.1021/nl404169a](https://doi.org/10.1021/nl404169a); pmid: [24299122](https://pubmed.ncbi.nlm.nih.gov/24299122/)
40. N. M. Schneider *et al.*, Electron–water interactions and implications for liquid cell electron microscopy. *J. Phys. Chem. C* **118**, 22373–22382 (2014). doi: [10.1021/jp507400n](https://doi.org/10.1021/jp507400n)
41. H. Zheng *et al.*, Observation of single colloidal platinum nanocrystal growth trajectories. *Science* **324**, 1309–1312 (2009). doi: [10.1126/science.1172104](https://doi.org/10.1126/science.1172104); pmid: [19498166](https://pubmed.ncbi.nlm.nih.gov/19498166/)
42. M. den Heijer, I. Shao, A. Radisic, M. C. Reuter, F. M. Ross, Patterned electrochemical deposition of copper using an electron beam. *APL Materials* **2**, 022101 (2014). doi: [10.1063/1.4863596](https://doi.org/10.1063/1.4863596)
43. E. Sutter *et al.*, In situ liquid-cell electron microscopy of silver-palladium galvanic replacement reactions on silver nanoparticles. *Nat. Commun.* **5**, 4946 (2014). doi: [10.1038/ncomms5946](https://doi.org/10.1038/ncomms5946); pmid: [25208691](https://pubmed.ncbi.nlm.nih.gov/25208691/)
44. A. Radisic, F. M. Ross, P. C. Seanson, In situ study of the growth kinetics of individual island electrodeposition of copper. *J. Phys. Chem. B* **110**, 7862–7868 (2006). doi: [10.1021/jp057549a](https://doi.org/10.1021/jp057549a); pmid: [16610883](https://pubmed.ncbi.nlm.nih.gov/16610883/)
45. A. Radisic, P. M. Vereecken, P. C. Seanson, F. M. Ross, The morphology and nucleation kinetics of copper islands during electrodeposition. *Surf. Sci.* **600**, 1817–1826 (2006). doi: [10.1016/j.susc.2006.02.025](https://doi.org/10.1016/j.susc.2006.02.025)
46. H. Zheng, S. A. Claridge, A. M. Minor, A. P. Alivisatos, U. Dahmen, Nanocrystal diffusion in a liquid thin film observed by in situ transmission electron microscopy. *Nano Lett.* **9**, 2460–2465 (2009). doi: [10.1021/nl9012369](https://doi.org/10.1021/nl9012369); pmid: [19408927](https://pubmed.ncbi.nlm.nih.gov/19408927/)
47. N. de Jonge, D. B. Peckys, G. J. Kremers, D. W. Piston, Electron microscopy of whole cells in liquid with nanometer resolution. *Proc. Natl. Acad. Sci. U.S.A.* **106**, 2159–2164 (2009). doi: [10.1073/pnas.0809567106](https://doi.org/10.1073/pnas.0809567106); pmid: [19164524](https://pubmed.ncbi.nlm.nih.gov/19164524/)
48. M. Sun, H.-G. Liao, K. Niu, H. Zheng, Structural and morphological evolution of lead dendrites during electrochemical migration. *Sci. Rep.* **3**, 3227 (2013). doi: [10.1038/sr13151](https://doi.org/10.1038/sr13151); pmid: [24233151](https://pubmed.ncbi.nlm.nih.gov/24233151/)
49. Z. Zeng *et al.*, Visualization of electrode-electrolyte interfaces in LiPF<sub>6</sub>/EC/DEC electrolyte for lithium ion batteries via in situ TEM. *Nano Lett.* **14**, 1745–1750 (2014). doi: [10.1021/nl403922u](https://doi.org/10.1021/nl403922u); pmid: [24443941](https://pubmed.ncbi.nlm.nih.gov/24443941/)
50. B. L. Mehdi *et al.*, Observation and quantification of nanoscale processes in lithium batteries by operando electrochemical (S)TEM. *Nano Lett.* **15**, 2168–2173 (2015). doi: [10.1021/acs.nanolett.5b00175](https://doi.org/10.1021/acs.nanolett.5b00175); pmid: [25705928](https://pubmed.ncbi.nlm.nih.gov/25705928/)
51. N. M. Schneider *et al.*, Visualization of active and passive control of morphology during electrodeposition. *Microsc. Microanal.* **20**, 1530–1531 (2014). doi: [10.1017/S14319276140009386](https://doi.org/10.1017/S14319276140009386)
52. B. L. Mehdi *et al.*, In-situ electrochemical transmission electron microscopy for battery research. *Microsc. Microanal.* **20**, 484–492 (2014). doi: [10.1017/S1431927614000488](https://doi.org/10.1017/S1431927614000488); pmid: [24755142](https://pubmed.ncbi.nlm.nih.gov/24755142/)
53. M. Gu *et al.*, Demonstration of an electrochemical liquid cell for operando transmission electron microscopy observation of the lithiation/delithiation behavior of Si nanowire battery anodes. *Nano Lett.* **13**, 6106–6112 (2013). doi: [10.1021/nl403402q](https://doi.org/10.1021/nl403402q); pmid: [24224495](https://pubmed.ncbi.nlm.nih.gov/24224495/)
54. R. L. Sacci *et al.*, Direct visualization of initial SEI morphology and growth kinetics during lithium deposition by in situ electrochemical transmission electron microscopy. *Chem. Commun. (Camb.)* **50**, 2104–2107 (2014). doi: [10.1039/c3cc49029g](https://doi.org/10.1039/c3cc49029g); pmid: [24413070](https://pubmed.ncbi.nlm.nih.gov/24413070/)
55. P. Abellan *et al.*, Probing the degradation mechanisms in electrolyte solutions for Li-ion batteries by in situ transmission electron microscopy. *Nano Lett.* **14**, 1293–1299 (2014). doi: [10.1021/nl404271k](https://doi.org/10.1021/nl404271k); pmid: [24559146](https://pubmed.ncbi.nlm.nih.gov/24559146/)
56. S. W. Chee, D. J. Duquette, F. M. Ross, R. Hull, Metastable structures in Al thin films prior to the onset of corrosion pitting as observed using liquid cell transmission electron microscopy. *Microsc. Microanal.* **20**, 462–468 (2014). doi: [10.1017/S1431927614000221](https://doi.org/10.1017/S1431927614000221); pmid: [24565052](https://pubmed.ncbi.nlm.nih.gov/24565052/)
57. S. W. Chee *et al.*, Studying localized corrosion using liquid cell transmission electron microscopy. *Chem. Commun.* **51**, 168–171 (2015). doi: [10.1039/C4CC06443G](https://doi.org/10.1039/C4CC06443G); pmid: [25388023](https://pubmed.ncbi.nlm.nih.gov/25388023/)
58. X. Zhong, M. G. Burke, S. Schilling, S. J. Haigh, N. J. Zaluzec, Novel hybrid sample preparation method for in situ liquid cell TEM analysis. *Microsc. Microanal.* **20** (suppl. S3), 1514–1515 (2014). doi: [10.1017/S14319276140009301](https://doi.org/10.1017/S14319276140009301); pmid: [25010485](https://pubmed.ncbi.nlm.nih.gov/25010485/)
59. H. G. Liao, L. Cui, S. Whitlam, H. Zheng, Real-time imaging of Pt<sub>3</sub>Fe nanorod growth in solution. *Science* **336**, 1011–1014 (2012). doi: [10.1126/science.1219185](https://doi.org/10.1126/science.1219185); pmid: [22628649](https://pubmed.ncbi.nlm.nih.gov/22628649/)
60. H. G. Liao, H. Zheng, Liquid cell transmission electron microscopy study of platinum iron nanocrystal growth and shape evolution. *J. Am. Chem. Soc.* **135**, 5038–5043 (2013). doi: [10.1021/ja310612p](https://doi.org/10.1021/ja310612p); pmid: [23477794](https://pubmed.ncbi.nlm.nih.gov/23477794/)
61. T. J. Woehl *et al.*, Direct observation of aggregative nanoparticle growth: Kinetic modeling of the size distribution and growth rate. *Nano Lett.* **14**, 373–378 (2014). doi: [10.1021/nl4043328](https://doi.org/10.1021/nl4043328); pmid: [24325680](https://pubmed.ncbi.nlm.nih.gov/24325680/)
62. K. L. Jungjohann, S. Bliznakov, P. W. Sutter, E. A. Stach, E. A. Sutter, In situ liquid cell electron microscopy of the solution growth of Au-Pd core-shell nanostructures. *Nano Lett.* **13**, 2964–2970 (2013). doi: [10.1021/nl4014277](https://doi.org/10.1021/nl4014277); pmid: [23721080](https://pubmed.ncbi.nlm.nih.gov/23721080/)
63. A. De Clercq *et al.*, Growth of Pt-Pd nanoparticles studied in situ by HRTEM in a liquid cell. *J. Phys. Chem. Lett.* **5**, 2126–2130 (2014). doi: [10.1021/jz500690a](https://doi.org/10.1021/jz500690a); pmid: [26270503](https://pubmed.ncbi.nlm.nih.gov/26270503/)
64. T. J. Woehl, J. E. Evans, I. Arslan, W. D. Ristenpart, N. D. Browning, Direct in situ determination of the mechanisms controlling nanoparticle nucleation and growth. *ACS Nano* **6**, 8599–8610 (2012). doi: [10.1021/nm303371g](https://doi.org/10.1021/nm303371g); pmid: [22957797](https://pubmed.ncbi.nlm.nih.gov/22957797/)
65. C. Park, T. J. Woehl, J. E. Evans, N. D. Browning, Minimum cost multi-way data association for optimizing multitarget tracking of interacting objects. *IEEE Trans. Pattern Anal. Mach. Intell.* **37**, 611–624 (2015). doi: [10.1109/TPAMI.2014.2346202](https://doi.org/10.1109/TPAMI.2014.2346202); pmid: [26353265](https://pubmed.ncbi.nlm.nih.gov/26353265/)
66. L. R. Parent *et al.*, Direct in situ observation of nanoparticle synthesis in a liquid crystal surfactant template. *ACS Nano* **6**, 3589–3596 (2012). doi: [10.1021/nm300671g](https://doi.org/10.1021/nm300671g); pmid: [22439964](https://pubmed.ncbi.nlm.nih.gov/22439964/)

67. T. Kraus, N. de Jonge, Dendritic gold nanowire growth observed in liquid with transmission electron microscopy. *Langmuir* **29**, 8427–8432 (2013). doi: [10.1021/la401584z](https://doi.org/10.1021/la401584z); pmid: [23789977](https://pubmed.ncbi.nlm.nih.gov/23789977/)
68. G. Zhu et al., In situ study of the growth of two-dimensional palladium dendritic nanostructures using liquid-cell electron microscopy. *Chem. Commun.* **50**, 9447–9450 (2014). doi: [10.1039/C4CC03500C](https://doi.org/10.1039/C4CC03500C); pmid: [24938863](https://pubmed.ncbi.nlm.nih.gov/24938863/)
69. Y. Jiang et al., In situ study of oxidative etching of palladium nanocrystals by liquid cell electron microscopy. *Nano Lett.* **14**, 3761–3765 (2014). doi: [10.1021/nl500670q](https://doi.org/10.1021/nl500670q); pmid: [24927485](https://pubmed.ncbi.nlm.nih.gov/24927485/)
70. J. Wu, W. Gao, H. Yang, J.-M. Zuo, Imaging shape-dependent corrosion behavior of Pt nanoparticles over extended time using a liquid flow cell and TEM. *Microsc. Microanal.* **20**, 1508–1509 (2014). doi: [10.1017/S1431927614009271](https://doi.org/10.1017/S1431927614009271)
71. K. W. Noh, Y. Liu, L. Sun, S. J. Dillon, Challenges associated with in-situ TEM in environmental systems: The case of silver in aqueous solutions. *Ultramicroscopy* **116**, 34–38 (2012). doi: [10.1016/j.ultramic.2012.03.012](https://doi.org/10.1016/j.ultramic.2012.03.012)
72. Y. Liu, K. Tai, S. J. Dillon, Growth kinetics and morphological evolution of ZnO precipitated from solution. *Chem. Mater.* **25**, 2927–2933 (2013). doi: [10.1021/cm303522z](https://doi.org/10.1021/cm303522z)
73. J. E. Evans, K. L. Jungjohann, N. D. Browning, I. Arslan, Controlled growth of nanoparticles from solution with in situ liquid transmission electron microscopy. *Nano Lett.* **11**, 2809–2813 (2011). doi: [10.1021/nl201166g](https://doi.org/10.1021/nl201166g); pmid: [21619024](https://pubmed.ncbi.nlm.nih.gov/21619024/)
74. K.-Y. Niu, J. Park, H. Zheng, A. P. Alivisatos, Revealing bismuth oxide hollow nanoparticle formation by the Kirkendall effect. *Nano Lett.* **13**, 5715–5719 (2013). doi: [10.1021/nl403536z](https://doi.org/10.1021/nl403536z); pmid: [24131312](https://pubmed.ncbi.nlm.nih.gov/24131312/)
75. H. L. Xin, H. Zheng, In situ observation of oscillatory growth of bismuth nanoparticles. *Nano Lett.* **12**, 1470–1474 (2012). doi: [10.1021/nl2041854](https://doi.org/10.1021/nl2041854); pmid: [22313455](https://pubmed.ncbi.nlm.nih.gov/22313455/)
76. H. Zheng, U. M. Mirsaidov, L. W. Wang, P. Matsudaira, Electron beam manipulation of nanoparticles. *Nano Lett.* **12**, 5644–5648 (2012). doi: [10.1021/nl302788g](https://doi.org/10.1021/nl302788g); pmid: [23035740](https://pubmed.ncbi.nlm.nih.gov/23035740/)
77. D. Li et al., Direction-specific interactions control crystal growth by oriented attachment. *Science* **336**, 1014–1018 (2012). doi: [10.1126/science.1219643](https://doi.org/10.1126/science.1219643); pmid: [22628650](https://pubmed.ncbi.nlm.nih.gov/22628650/)
78. J. M. Grogan, L. Rotkina, H. H. Bau, In situ liquid-cell electron microscopy of colloid aggregation and growth dynamics. *Phys. Rev. E Stat. Nonlin. Soft Matter Phys.* **83**, 061405 (2011). doi: [10.1103/PhysRevE.83.061405](https://doi.org/10.1103/PhysRevE.83.061405); pmid: [21797362](https://pubmed.ncbi.nlm.nih.gov/21797362/)
79. J. Park et al., Direct observation of nanoparticle superlattice formation by using liquid cell transmission electron microscopy. *ACS Nano* **6**, 2078–2085 (2012). doi: [10.1021/nl203837m](https://doi.org/10.1021/nl203837m); pmid: [22360715](https://pubmed.ncbi.nlm.nih.gov/22360715/)
80. D. Bhattacharya, M. Bosman, V. R. S. S. Mokkaipati, F. Y. Leong, U. Mirsaidov, Nucleation dynamics of water nanodroplets. *Microsc. Microanal.* **20**, 407–415 (2014). doi: [10.1017/S1431927614000476](https://doi.org/10.1017/S1431927614000476); pmid: [24667092](https://pubmed.ncbi.nlm.nih.gov/24667092/)
81. C.-Y. Ruan, V. A. Lobastov, F. Vigliotti, S. Chen, A. H. Zewail, Ultrafast electron crystallography of interfacial water. *Science* **304**, 80–84 (2004). doi: [10.1126/science.1094818](https://doi.org/10.1126/science.1094818); pmid: [15064414](https://pubmed.ncbi.nlm.nih.gov/15064414/)
82. N. D. Browning et al., Recent developments in dynamic transmission electron microscopy. *Curr. Opin. Solid State Mater. Sci.* **16**, 23–30 (2012). doi: [10.1016/j.cossms.2011.07.001](https://doi.org/10.1016/j.cossms.2011.07.001)
83. U. Mirsaidov, C.-D. Ohl, P. Matsudaira, A direct observation of nanometer-size void dynamics in an ultra-thin water film. *Soft Matter* **8**, 7108–7111 (2012). doi: [10.1039/c2sm25331c](https://doi.org/10.1039/c2sm25331c)
84. U. M. Mirsaidov, H. Zheng, D. Bhattacharya, Y. Casana, P. Matsudaira, Direct observation of stick-slip movements of water nanodroplets induced by an electron beam. *Proc. Natl. Acad. Sci. U.S.A.* **109**, 7187–7190 (2012). doi: [10.1073/pnas.1200457109](https://doi.org/10.1073/pnas.1200457109); pmid: [22517747](https://pubmed.ncbi.nlm.nih.gov/22517747/)
85. M. M. Norton, F. M. Ross, H. H. Bau, Nano bubble migration in a tapered conduit in the asymptotic limits of zero capillary and bond numbers: Theory and experiments. *Bull. Am. Phys. Soc.* **60**, H36.00004 (2015). <http://meetings.aps.org/Meeting/DFD15/Session/H36.4>
86. D. Mattia, Y. Gogotsi, Review: Static and dynamic behavior of liquids inside carbon nanotubes. *Microfluidics Nanofluidics* **5**, 289–305 (2008). doi: [10.1007/s10404-008-0293-5](https://doi.org/10.1007/s10404-008-0293-5)
87. U. Mirsaidov et al., Scrolling graphene into nanofluidic channels. *Lab Chip* **13**, 2874–2878 (2013). doi: [10.1039/c3lc50304f](https://doi.org/10.1039/c3lc50304f); pmid: [23702655](https://pubmed.ncbi.nlm.nih.gov/23702655/)
88. E. A. Ring, N. de Jonge, Video-frequency scanning transmission electron microscopy of moving gold nanoparticles in liquid. *Micron* **43**, 1078–1084 (2012). doi: [10.1016/j.micron.2012.01.010](https://doi.org/10.1016/j.micron.2012.01.010); pmid: [22386765](https://pubmed.ncbi.nlm.nih.gov/22386765/)
89. E. R. White, M. Mecklenburg, B. Shevitski, S. B. Singer, B. C. Regan, Charged nanoparticle dynamics in water induced by scanning transmission electron microscopy. *Langmuir* **28**, 3695–3698 (2012). doi: [10.1021/la204848g](https://doi.org/10.1021/la204848g); pmid: [22320230](https://pubmed.ncbi.nlm.nih.gov/22320230/)
90. J. Lu, Z. Aabdin, N. D. Loh, D. Bhattacharya, U. Mirsaidov, Nanoparticle dynamics in a nanodroplet. *Nano Lett.* **14**, 2111–2115 (2014). doi: [10.1021/nl500766j](https://doi.org/10.1021/nl500766j); pmid: [24641092](https://pubmed.ncbi.nlm.nih.gov/24641092/)
91. P.-A. Cazade, R. Hartkamp, B. Coasne, Structure and dynamics of an electrolyte confined in charged nanopores. *J. Phys. Chem. C* **118**, 5061–5072 (2014). doi: [10.1021/jp4098638](https://doi.org/10.1021/jp4098638)
92. S. Kashyap, T. J. Woehl, X. Liu, S. K. Mallapragada, T. Prozorov, Nucleation of iron oxide nanoparticles mediated by Mms6 protein in situ. *ACS Nano* **8**, 9097–9106 (2014). doi: [10.1021/nl502551y](https://doi.org/10.1021/nl502551y); pmid: [25162493](https://pubmed.ncbi.nlm.nih.gov/25162493/)
93. M. H. Nielsen, J. R. I. Lee, Q. N. Hu, T. Y. J. Han, J. J. De Yoreo, Structural evolution, formation pathways and energetic controls during template-directed nucleation of CaCO<sub>3</sub>. *Faraday Discuss.* **159**, 105–121 (2012). doi: [10.1039/c2fd20050c](https://doi.org/10.1039/c2fd20050c)
94. M. H. Nielsen, S. Aloni, J. J. De Yoreo, In situ TEM imaging of CaCO<sub>3</sub> nucleation reveals coexistence of direct and indirect pathways. *Science* **345**, 1158–1162 (2014). pmid: [25190792](https://pubmed.ncbi.nlm.nih.gov/25190792/)
95. P. J. M. Smeets, K. R. Cho, R. G. E. Kempen, N. A. J. M. Sommerdijk, J. J. De Yoreo, Calcium carbonate nucleation driven by ion binding in a biomimetic matrix revealed by in situ electron microscopy. *Nat. Mater.* **14**, 394–399 (2015). doi: [10.1038/nmat4193](https://doi.org/10.1038/nmat4193); pmid: [25622001](https://pubmed.ncbi.nlm.nih.gov/25622001/)
96. T. J. Woehl et al., Correlative electron and fluorescence microscopy of magnetotactic bacteria in liquid: Toward in vivo imaging. *Sci. Rep.* **4**, 6854 (2014). doi: [10.1038/srep06854](https://doi.org/10.1038/srep06854); pmid: [25358460](https://pubmed.ncbi.nlm.nih.gov/25358460/)
97. D. B. Peckys, N. de Jonge, Visualizing gold nanoparticle uptake in live cells with liquid scanning transmission electron microscopy. *Nano Lett.* **11**, 1733–1738 (2011). doi: [10.1021/nl200285r](https://doi.org/10.1021/nl200285r); pmid: [21410218](https://pubmed.ncbi.nlm.nih.gov/21410218/)
98. E. A. Ring, D. B. Peckys, M. J. Dukes, J. P. Baudoin, N. de Jonge, Silicon nitride windows for electron microscopy of whole cells. *J. Microsc.* **243**, 273–283 (2011). doi: [10.1111/j.1365-2818.2011.03501.x](https://doi.org/10.1111/j.1365-2818.2011.03501.x); pmid: [21770941](https://pubmed.ncbi.nlm.nih.gov/21770941/)
99. M. J. Dukes, D. B. Peckys, N. de Jonge, Correlative fluorescence microscopy and scanning transmission electron microscopy of quantum-dot-labeled proteins in whole cells in liquid. *ACS Nano* **4**, 4110–4116 (2010). doi: [10.1021/nl101023z](https://doi.org/10.1021/nl101023z); pmid: [20550177](https://pubmed.ncbi.nlm.nih.gov/20550177/)
100. D. B. Peckys, U. Korf, N. de Jonge, Local variations of HER2 dimerization in breast cancer cells discovered by correlative fluorescence and liquid electron microscopy. *Sci. Advances* **1**, e1500165 (2015). doi: [10.1126/sciadv.1500165](https://doi.org/10.1126/sciadv.1500165)
101. D. B. Peckys, J.-P. Baudoin, M. Eder, U. Werner, N. de Jonge, Epidermal growth factor receptor subunit locations determined in hydrated cells with environmental scanning electron microscopy. *Scientific Reports* **3**, 2626 (2013). doi: [10.1038/srep02626](https://doi.org/10.1038/srep02626); pmid: [24022088](https://pubmed.ncbi.nlm.nih.gov/24022088/)
102. E. S. Pohlmann et al., Real-time visualization of nanoparticles interacting with glioblastoma stem cells. *Nano Lett.* **15**, 2329–2335 (2015). doi: [10.1021/nl504481k](https://doi.org/10.1021/nl504481k); pmid: [25734907](https://pubmed.ncbi.nlm.nih.gov/25734907/)
103. D. B. Peckys, N. de Jonge, Liquid scanning transmission electron microscopy: Imaging protein complexes in their native environment in whole eukaryotic cells. *Microsc. Microanal.* **20**, 346–365 (2014). doi: [10.1017/S1431927614000099](https://doi.org/10.1017/S1431927614000099); pmid: [24548636](https://pubmed.ncbi.nlm.nih.gov/24548636/)
104. Q. Chen et al., 3D motion of DNA-Au nanoconjugates in graphene liquid cell electron microscopy. *Nano Lett.* **13**, 4556–4561 (2013). doi: [10.1021/nl402694n](https://doi.org/10.1021/nl402694n); pmid: [23944844](https://pubmed.ncbi.nlm.nih.gov/23944844/)
105. N. Mohanty, M. Fahrenholtz, A. Nagaraja, D. Boyle, V. Berry, Impermeable graphenic encasement of bacteria. *Nano Lett.* **11**, 1270–1275 (2011). doi: [10.1021/nl104292k](https://doi.org/10.1021/nl104292k); pmid: [21271738](https://pubmed.ncbi.nlm.nih.gov/21271738/)
106. J. Park et al., Direct observation of wet biological samples by graphene liquid cell transmission electron microscopy. *Nano Lett.* **15**, 4737–4744 (2015). doi: [10.1021/acs.nanolett.5b01636](https://doi.org/10.1021/acs.nanolett.5b01636); pmid: [26065925](https://pubmed.ncbi.nlm.nih.gov/26065925/)
107. C. Wang, Q. Qiao, T. Shokuhfar, R. F. Klie, High-resolution electron microscopy and spectroscopy of ferritin in biocompatible graphene liquid cells and graphene sandwiches. *Adv. Mater.* **26**, 3410–3414 (2014). doi: [10.1002/adma.201306069](https://doi.org/10.1002/adma.201306069); pmid: [24497051](https://pubmed.ncbi.nlm.nih.gov/24497051/)
108. S. M. Hoppe, D. Y. Sasaki, A. N. Kinghorn, K. Hattar, In-situ transmission electron microscopy of liposomes in an aqueous environment. *Langmuir* **29**, 9958–9961 (2013). doi: [10.1021/la401288g](https://doi.org/10.1021/la401288g); pmid: [23886420](https://pubmed.ncbi.nlm.nih.gov/23886420/)
109. M. T. Proetto et al., Dynamics of soft nanomaterials captured by transmission electron microscopy in liquid water. *J. Am. Chem. Soc.* **136**, 1162–1165 (2014). doi: [10.1021/ja408513m](https://doi.org/10.1021/ja408513m); pmid: [24422495](https://pubmed.ncbi.nlm.nih.gov/24422495/)
110. F. A. Plamper et al., Spontaneous assembly of miktoarm stars into vesicular interpolyelectrolyte complexes. *Macromol. Rapid Commun.* **34**, 855–860 (2013). doi: [10.1002/marc.201300053](https://doi.org/10.1002/marc.201300053); pmid: [23508924](https://pubmed.ncbi.nlm.nih.gov/23508924/)
111. M. Wojcik, M. Hauser, W. Li, S. Moon, K. Xu, Graphene-enabled electron microscopy and correlated super-resolution microscopy of wet cells. *Nat. Commun.* **6**, 7384 (2015). doi: [10.1038/ncomms8384](https://doi.org/10.1038/ncomms8384); pmid: [26066680](https://pubmed.ncbi.nlm.nih.gov/26066680/)
112. A. Fukami, K. Fukushima, N. Kohyama, Observation technique for wet clay minerals using film-sealed environmental cell equipment attached to high-resolution electron microscope, in *Microstructure of Fine-Grained Sediments*, R. Bennett et al., Eds. (Springer New York, 1991), pp. 321–331.
113. K. Adachi, E. J. Freney, P. R. Buseck, Shapes of internally mixed hygroscopic aerosol particles after deliquescence, and their effect on light scattering. *Geophys. Res. Lett.* **38**, L13804 (2011). doi: [10.1029/2011GL047540](https://doi.org/10.1029/2011GL047540)
114. P. G. de Gennes, Wetting: Statics and dynamics. *Rev. Mod. Phys.* **57**, 827–863 (1985). doi: [10.1103/RevModPhys.57.827](https://doi.org/10.1103/RevModPhys.57.827)
115. S. Sadiq, P. Schottland, N. Brodie, G. Sabouraud, The mechanisms of pyrrole electropolymerization. *Chem. Soc. Rev.* **29**, 283–293 (2000). doi: [10.1039/a807124a](https://doi.org/10.1039/a807124a)
116. S. Helveg et al., Atomic-scale imaging of carbon nanofiber growth. *Nature* **427**, 426–429 (2004). doi: [10.1038/nature02278](https://doi.org/10.1038/nature02278); pmid: [14749826](https://pubmed.ncbi.nlm.nih.gov/14749826/)
117. B. K. Miller, P. A. Crozier, Analysis of catalytic gas products using electron energy-loss spectroscopy and residual gas analysis for operando transmission electron microscopy. *Microsc. Microanal.* **20**, 815–824 (2014). doi: [10.1017/S1431927614000749](https://doi.org/10.1017/S1431927614000749); pmid: [24815065](https://pubmed.ncbi.nlm.nih.gov/24815065/)
118. P. L. Gai, Development of wet environment TEM (wet-ETEM) for in situ studies of liquid-catalyst reactions on the nanoscale. *Microsc. Microanal.* **8**, 21–28 (2002). doi: [10.1017/S143192760201005x](https://doi.org/10.1017/S143192760201005x); pmid: [14710723](https://pubmed.ncbi.nlm.nih.gov/14710723/)
119. F. M. Ross, Controlling nanowire structures through real time growth studies. *Rep. Prog. Phys.* **73**, 114501–114522 (2010). doi: [10.1088/0034-4885/73/11/114501](https://doi.org/10.1088/0034-4885/73/11/114501)
120. R. Danev, K. Nagayama, Transmission electron microscopy with Zernike phase plate. *Ultramicroscopy* **88**, 243–252 (2001). doi: [10.1016/S0304-3991\(01\)00088-2](https://doi.org/10.1016/S0304-3991(01)00088-2); pmid: [11545320](https://pubmed.ncbi.nlm.nih.gov/11545320/)
121. P. Simon et al., Electron holography of biological samples. *Micron* **39**, 229–256 (2008). doi: [10.1016/j.micron.2006.11.012](https://doi.org/10.1016/j.micron.2006.11.012); pmid: [17374487](https://pubmed.ncbi.nlm.nih.gov/17374487/)

## ACKNOWLEDGMENTS

The research described in this review was partially supported by the National Science Foundation under NSF-GOALI grants DMR-1310639 and CMMI-1129722. I acknowledge A. W. Ellis and M. C. Reuter of IBM for their technical assistance with the development of the liquid cell technique.

10.1126/science.aaa9886